Biomacromolecules

Article

Cite This: Biomacromolecules 2018, 19, 1592−1601

pubs.acs.org/Biomac

Synthesis and Characterization of Temperature-Sensitive and Chemically Cross-Linked Poly(*N*-isopropylacrylamide)/Photosensitizer Hydrogels for Applications in Photodynamic Therapy

Simin Belali,[†,‡] Huguette Savoie,[§] Jessica M. O'Brien,[†] Atillio A. Cafolla,[∥] Barry O'Connell,[⊥] Ali Reza Karimi,[‡] Ross W. Boyle,[§] and Mathias O. Senge*[,†,#]

[†]School of Chemistry, SFI Tetrapyrrole Laboratory, Trinity Biomedical Science Institute, Trinity College Dublin, the University of Dublin, 152-160 Pearse Street, Dublin 2, Ireland

[‡]Department of Chemistry, Faculty of Science, Arak University, Arak 38156-8-8349, Iran

[§]Department of Chemistry, University of Hull, Cottingham Road, Kingston-upon-Hull HU6 7RX, United Kingdom

[∥]School of Physical Sciences and [⊥]Nano Research Facility, Dublin City University, Glasnevin, Dublin 9, Ireland

[#]Medicinal Chemistry, Trinity Translational Medicine Institute, Trinity Centre for Health Sciences, Trinity College Dublin, the University of Dublin, St. James's Hospital, Dublin 8, Ireland

Supporting Information

ABSTRACT: A novel poly(*N*-isopropylacrylamide) (PNIPAM) hydrogel containing different photosensitizers (protoporphyrin IX (PpIX), pheophorbide a (Pba), and protoporphyrin IX dimethyl ester (PpIX-DME)) has been synthesized with a significant improvement in water solubility and potential for PDT applications compared to the individual photosensitizers (PSs). Conjugation of PpIX, Pba, and PpIX-DME to the poly(*N*-isopropylacrylamide) chain was achieved using the dispersion polymerization method. This study describes how the use of nanohydrogel structures to deliver a photosensitizer with low water solubility and high aggregation tendencies in polar solvents overcomes these limitations. FT-IR spectroscopy, UV−vis spectroscopy, ^{1}H NMR, fluorescence spectroscopy, SEM, and DLS analysis were used to characterize the PNIPAM−photosensitizer nanohydrogels. Spectroscopic studies indicate that the PpIX, Pba, and PpIX-DME photosensitizers are covalently conjugated to the polymer chains, which prevents aggregation and thus allows significant singlet oxygen production upon illumination. Likewise, the lower critical solution temperature was raised to ∼44 °C in the new PNIPAM-PS hydrogels. The PNIPAM hydrogels are biocompatible with >90% cell viability even at high concentrations of the photosensitizer *in vitro*. Furthermore, a very sharp onset of light-dependent toxicity for the PpIX-based nanohydrogel in the nanomolar range and a more modest, but significant, photocytotoxic response for Pba-PNIPAM and PpIX-DME-PNIPAM nanohydrogels suggest that the new hydrogels have potential for applications in photodynamic therapy.

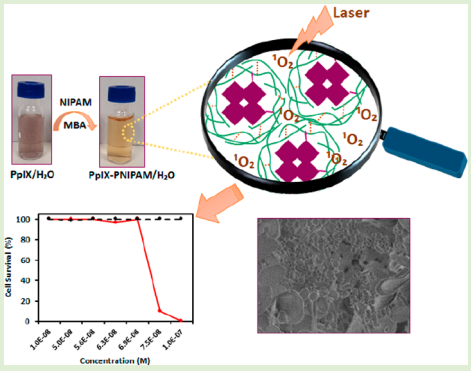

INTRODUCTION

Photodynamic therapy (PDT) relies on the activation of a photosensitizer (PS) using visible or near-IR light to generate reactive oxygen species, such as singlet oxygen, as cytotoxic agents.[1,2] Porphyrins feature prominently among the clinically approved PDT drugs and typical examples of porphyrin-based drugs include Photofrin (porfimer sodium), Visudyne (verteporfin), and Foscan (temoporfin).[2,3] A recurring problem is the intrinsically low water solubility of many porphyrinoid PSs and their tendency to aggregate in polar solvents and biological media. Aggregation results in quenching of the excited states, thus lowering the singlet oxygen yields and impacts the ability of a PS to reach the target tissue limiting its clinical use. In order to overcome these limitations and to obviate side effects, different strategies to improve the pharmacological profile of PSs have been developed.[4] In terms of approved drugs this mostly involves liposomal formulations (Visudyne), polar functionalities in the PS (Photofrin), or the use of biosynthetic precursors (Levulan). This is complemented by a range of nanomedicinal strategies, incorporation of water-soluble side chains, or other formulation techniques for second- and third-generation PSs.[5,6]

In terms of biocompatibility, the natural protoporphyrin IX (PpIX) would be a good PDT drug candidate.[7] Currently, it is only used clinically via application of its biosynthetic precursor 5-aminolevulinic acid (Levulan or its methyl ester, Metvixia) as

Received: February 19, 2018
Revised: March 13, 2018
Published: March 29, 2018

DOI: 10.1021/acs.biomac.8b00293
Biomacromolecules 2018, 19, 1592−1601

a pro-drug. PpIX can be an effective photosensitizer for PDT application as shown by its effect in ALA-induced PDT.[8] However, PpIX "as is" is not suitable for direct intravenous injection due to its low water solubility and tendency for aggregation. This aggregation in water is due to π-stacking interactions and edge-to-edge hydrophobic interactions. In addition, intermolecular hydrogen bonds between the carboxylic acid groups stabilize porphyrin aggregates.[9] Aggregation poses a problem as it leads to accumulation in skin and prolonged light sensitivity, undermines the efficiency of singlet oxygen production, and reduces treatment efficacy.[10] Similar arguments pertain to the use pheophorbide a (Pba), a key test compound[11] for the use of chlorophyll derivatives in PDT.[3,12,13] Again, low water solubility and lack of selectivity often cause accidental damage to normal cells and long-term cutaneous photosensitivity.[14,15]

Clearly, there is a need to provide a simple solution that will improve the solubility and stability of standard photosensitizers (such as PpIX, Pba, and related compounds). Most of the standard strategies[4,5] for water solublization and stable formulations of photosensitizers use encapsulation in colloidal carriers,[16,17] nanoparticles,[5,18−20] and micelles[21] or drug formulation additives.[22] Yet, few reports deal with stable formulations of PpIX and Pba for systemic administration,[23,24] and these either use complex coupling chemistry or simple encapsulation which allows possible leakage of the PS.

Recently, hydrogels have attracted attention as a rather simple and facile means to solubilize and deliver drugs.[25] Hydrogels are three-dimensional hydrophilic, polymeric networks capable of absorbing large amounts of water or biological fluids. In the area of PDT a range of different PS−hydrogel materials have been prepared,[26,27] mostly using simple PS dyes, encapsulation, or copolymerization. The random distribution of cross-linkers or copolymers in the 3D network of the hydrogel not only prevents aggregation of the copolymer or cross-linker, but the highly macroporous networks also enable molecules and cells to enter and migrate freely throughout the material. Thus, hydrogels offer significant potential as injectable, water-soluble carriers for nonaggregated PSs with high singlet oxygen production.

A PS can be incorporated into a hydrogel either via simple noncovalent encapsulation or through copolymerization and covalent linkage. The former has the drawback of the PS leaking from the hydrogel with associated loss of activity. A facile approach uses the PS itself as the cross-linker in the hydrogel, as recently shown with an A_4-type porphyrin in a *N*-isopropylacrylamide (PNIPAM) hydrogel[28] and a BODIPY−cross-linked chitosan hydrogel.[29] These results prompted us to investigate whether key natural PSs such as protoporphyrin IX or pheophorbide a can be formulated in such a manner and to develop a simple means for their use in PDT and translational drug development. Herein we describe the direct use of protoporphyrin IX, protoporphyrin IX dimethyl ester (PPIX-DME), and pheophorbide a as the copolymer in PNIPAM hydrogels to yield stable, water-soluble nanohydrogels (Figure 1), in which the PSs remain active photosensitizers with excellent *in vitro* PDT efficacy.

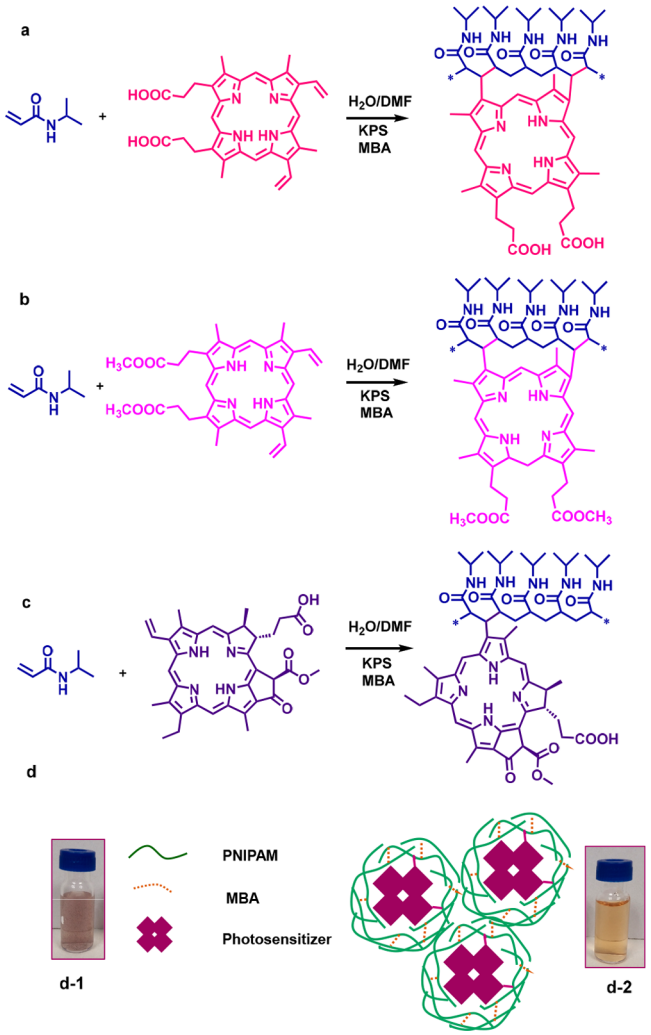

Figure 1. Schematic illustration of the preparation of (a) poly(*N*-isopropylacrylamide)−protoporphyrin IX (PpIX-PNIPAM), (b) poly(*N*-isopropylacrylamide)−pheophorbide a (Pba-PNIPAM), and (c) poly(*N*-isopropylacrylamide)−protoporphyrin IX dimethyl ester (PpIX-DME-PNIPAM) nanohydrogels. (d-1) Protoporphyrin IX as a dispersion in water and (d-2) PNIPAM-PpIX nanohydrogel showing complete solubility in aqueous media.

EXPERIMENTAL SECTION

Materials. *N*-Isopropylacrylamide (NIPAAM, 99%), methylenebis(acrylamide) (MBA, 99%), protoporphyrin IX (≥95%), and potassium persulfate (KPS, 99%) were purchased from Sigma-Aldrich. Poly(*N*-vinylpyrrolidone) 25 (PVP, average MW ~ 292.23 g mol^{-1}) was purchased from Merck. Deionized and distilled water was used for all solution preparations. Pheophorbide a[30] and PPIX-DME[31] were prepared as previously described.

Synthesis of Protoporphyrin IX−Poly(*N*-isopropylacrylamide) Nanohydrogel (PpIX-PNIPAM). The PpIX-PNIPAM hydrogels were synthesized using the *in situ* dispersion polymerization method in a mixture of water and dimethylformamide (DMF, as organic solvent for dissolution of protoporphyrin IX in the reaction mixture). In a typical procedure, NIPAM (2.65 mmol, 300 mg), *N*,*N*-methylenebis(acrylamide) (MBA) (0.1 mmol, 16 mg), and PVP (300 mg) were dissolved in 6 mL of deionized water, and PpIX (2% w/w, 6 mg, 3% w/w, 9 mg, or 4% w/w, 12 mg) was dissolved in DMF, with both solutions then mixed in a Schlenk tube under nitrogen gas. The solution was stirred at 350 rpm and heated to 70 °C for 40 min under continuous purging with a nitrogen atmosphere. The initiator, potassium persulfate (0.076 mmol, 200 mg), dissolved in 1.0 mL of deionized water, was added to the mixture to start polymerization. The reaction was carried out at 70 °C for 24 h under a N_2 atmosphere. After polymerization, to remove unreacted monomers from the resultant hydrogels, the products were dialyzed against deionized water using dialysis bags at room temperature for 2 days.

DOI: 10.1021/acs.biomac.8b00293
Biomacromolecules 2018, 19, 1592−1601

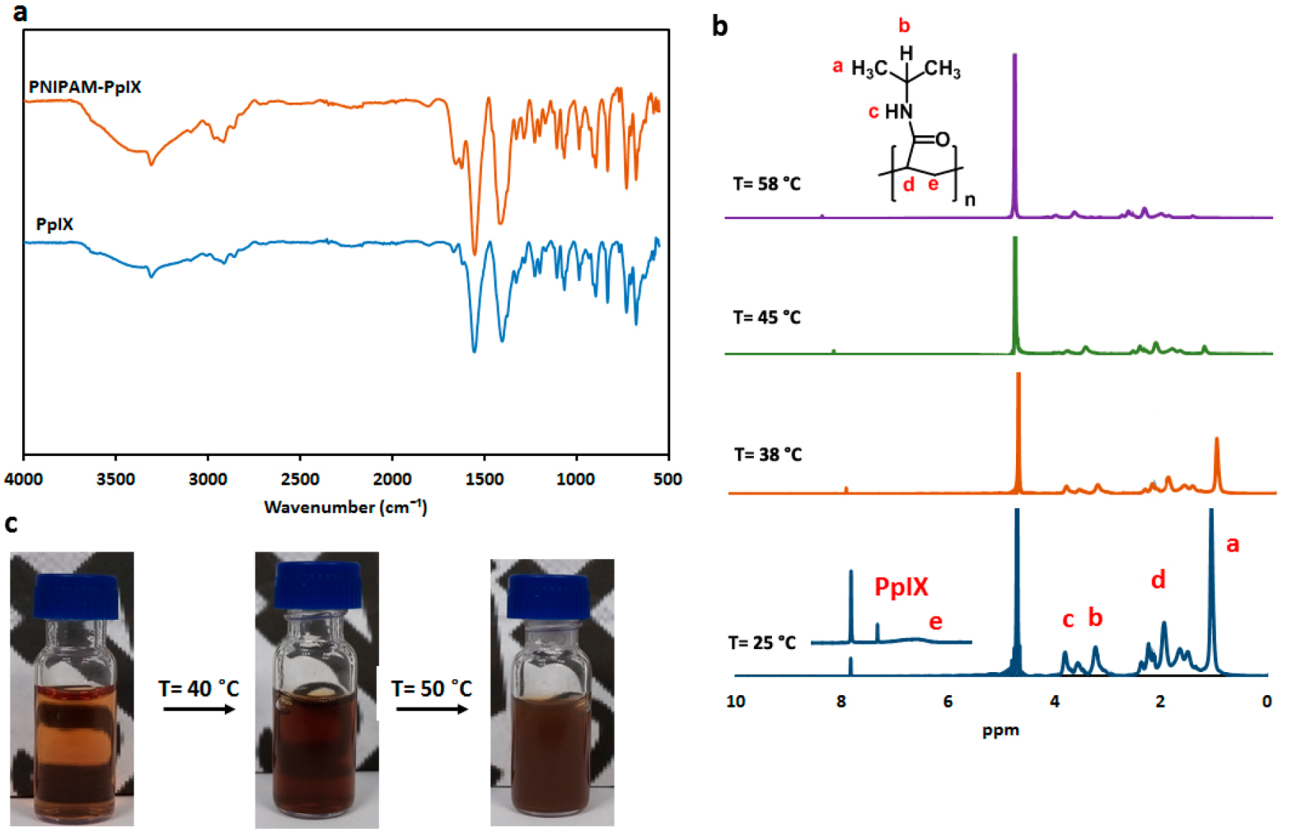

Figure 2. (a) FT-IR spectra of protoporphyrin IX and poly(*N*-isopropylacrylamide)−protoporphyrin IX hydrogel. (b) 600 MHz ^{1}H NMR spectra of PpIX-PNIPAM nanohydrogel in D_2O at different temperatures. (c) Pictorial illustration of the LCST type phase transition of the PpIX-PNIPAM nanohydrogel at 40 and 50 °C.

Synthesis of Protoporphyrin IX Dimethyl Ester−Poly(*N*-isopropylacrylamide) Nanohydrogels (PpIX-DME-PNIPAM). Preparation followed the method used for PpIX-PNIPAM using protoporphyrin IX dimethyl ester (3% w/w, 9 mg) in 4 mL of DMF.

Synthesis of Pheophorbide a−Poly(*N*-isopropylacrylamide) Nanohydrogel (Pba-PNIPAM). Preparation followed the method used for PpIX-PNIPAM using pheophorbide a (3% w/w, 9 mg) in 4 mL of DMF.

Physical Characterization. ^{1}H NMR spectra were recorded on a Bruker Advance III 400 MHz, a Bruker DPX400, or an Agilent 400 spectrometer. UV−vis spectra were recorded using a Specord 250 spectrophotometer from Analytic Jena (1 cm path length, quartz cell). Emission and excitation spectra were measured using a Cary Eclipse G9800A fluorescence spectrophotometer. Fourier transform infrared (FT-IR) measurements were performed with a Digilab FTS-6000 spectrometer. Particle size distributions were measured using dynamic light scattering (DLS; ZetaSizer 3000 HS, Malvern Instruments). Differential scanning calorimetry (DSC), using a PerkinElmer Diamond DSC instrument with a scan rate of 1 K min^{-1}, was used to determine the exact temperature of the LCST point. SEM images were taken on a Jeol JSM IT-100 instrument. The applied voltage on the cathode was 2 kV.

Singlet Oxygen Production. Photoirradiation experiments were performed in quartz cuvettes (2 × 1 × 1 cm) using a polychromatic light source (Philips, 15 V−150 W lamp), equipped with a 400 nm cutoff filter (Schott GG 400) and a 532 nm diode pumped solid state green laser system (CW532-04, average intensity of 10 mW cm^{-2}). The sample temperature was kept at 18 °C using a Peltier element (Cary Peltier 1 × 1 cell holder). Relative $^1O_2$ yields (Φ_Δ) were calculated from the slopes of the 1,3-diphenylisobenzofuran (DPBF) conversion in the presence of different photosensitizers. The decrease in UV absorbance (417 nm) of DPBF in the presence of PpIX-PNIPAM, Pba-PNIPAM, and PpIX-DME-PNIPAM hydrogels was measured in DMSO; 5,10,15,20-tetraphenylporphyrin (TPP) in DMSO was used as a standard. Equation 1 was used to calculate the singlet oxygen generation efficiency of the hydrogels.[32]

$$\eta_{\Delta\text{hydrogel}} = \Phi_{\text{TPP}} \frac{t_{\text{TPP}}}{t_{\text{hydrogel}}} \quad (1)$$

In this equation, t_{TPP} is the time for the decrease in absorption of DPBF in the presence of TPP in DMSO and t_{hydrogel} is the time for the decrease in absorption of DPBF in the presence of the individual hydrogels. Φ_{TPP} is the singlet oxygen quantum yield of TPP (0.52 ± 0.15).[33]

Photocytotoxicity Tests. Cell viability was used to investigate the cytotoxicity of the PpIX-PNIPAM, Pba-PNIPAM, and PpIX-DME-PNIPAM hydrogels for cancer cells (HT-29, human colon adenocarcinoma) using the MTT assay.[34] In brief, solutions of the hydrogels in DMSO were further diluted in DMEM medium (Dulbecco's Modified Eagle's Medium with 4.5 g L^{-1} glucose and 2 mM L-glutamine without FCS) to give a range of concentrations. The HT-29 cells were adjusted to a concentration of 1 × 10^6 cells/mL. 800 μL of this cell suspension was added to 200 μL of the dilutions at 5× the desired concentration and incubated in the dark for an hour at 37 °C and under 5% CO_2, after which they were washed in a 3-fold excess of medium to eliminate any unbound compound. The pellets of cells and compound were resuspended in 1 mL of medium, and 4 × 100 μL of each cell (8 × 10^4) and dye concentration was put into two 96-well plates. One plate was irradiated with white light (20 J cm^{-2} provided by an Oriel quartz tungsten halogen lamp housing model 66188 powered by an Oriel 1100 W radiometric power supply, model 69935) while the other served as a dark toxicity control. After irradiation, 5 μL of fetal bovine serum was added to each well, and the plates were returned to the incubator overnight. After 18−24 h, an MTT cell viability assay was performed, and the results were expressed as percent of cell viability versus compound concentration; an LD_{90}

DOI: 10.1021/acs.biomac.8b00293
Biomacromolecules 2018, 19, 1592−1601

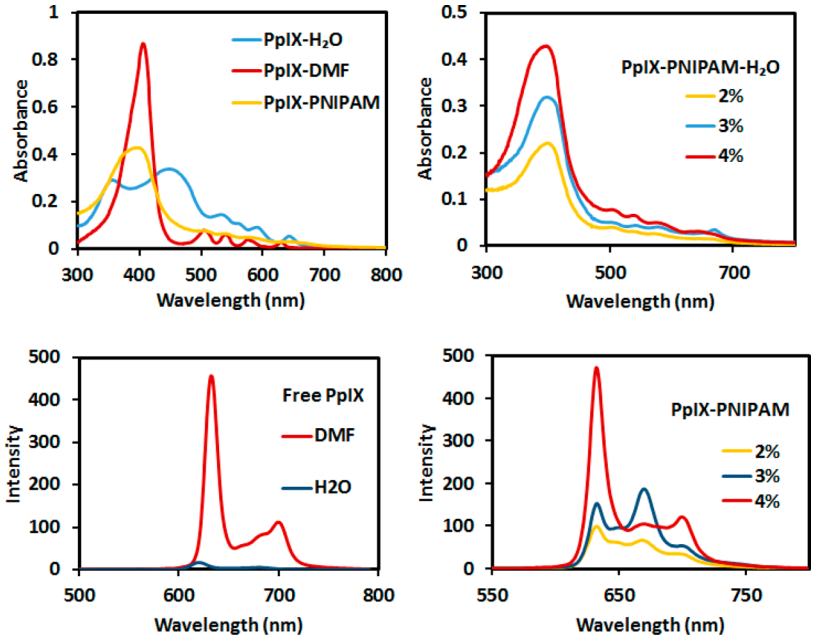

Figure 3. (a) UV−vis spectra of protoporphyrin IX (1.5×10^{-4} M) in H_2O and DMF (1.5×10^{-5} M) and PpIX-PNIPAM hydrogel (1.5×10^{-5} M) in H_2O. (b) Fluorescence emission spectra of PpIX in DMF and H_2O (λ_{ex} = 409 nm). (c) UV−vis absorption spectra of PpIX-PNIPAM hydrogel at different concentrations of protoporphyrin IX in the hydrogel structure (2%, 3%, and 4%) in H_2O (the concentration of PpIX in 4% PpIX-PNIPAM hydrogel = 1.5×10^{-5}, in 3% = 1.1×10^{-5}, and in 2% = 0.75×10^{-5} M. (d) Fluorescence spectra of PpIX-PNIPAM hydrogel (λ_{ex} = 409 nm) at different concentrations of protoporphyrin IX in H_2O.

(dose where 90% of the cells are killed) was determined from the resulting curves.

RESULTS AND DISCUSSION

Preparation and Characterization of PS−Nanohydrogels. The PpIX-PNIPAM hydrogel was synthesized using an *in situ* dispersion polymerization method which involves mixing organic (to handle the water-insoluble PS monomers) and aqueous solvents. The presence of a double bond in the *N*-isopropylacrylamide structure as the main monomer and the two vinyl groups in PpIX as the copolymer is key for the polymerization. The optimum concentration of PpIX in the hydrogel structure was established as 4 wt %; higher concentrations resulted in increased hydrophobicity of the hydrogel and a decrease in its solubility in aqueous media.

Initial structural characterization of PpIX-PNIPAM hydrogels involved FT-IR and ^{1}H NMR spectroscopy. The FT-IR spectra (Figure 2a) exhibit the typical amide I band, as indicated by the carbonyl stretch of PNIPAM at 1647 cm^{-1} and the amide II band shows the N−H vibration at 1550 cm^{-1}. Signals at 1372 and 1365 cm^{-1} were assigned to the methyl bending vibration of the symmetric isopropyl groups. In addition, the signal at 3281 cm^{-1} was attributed to the stretching vibration of the hydroxyl group of the acid in the hydrogel structure.

The ^{1}H NMR spectra of the hydrogel at different temperatures are shown in Figure 2b. Typical resonances attributable to the hydrogen atoms of the PNIPAM unit are clearly observed in the upfield area and the peaks in the downfield area are ascribed to the protoporphyrin IX section of the hydrogel structure. The ^{1}H NMR spectrum at 25 °C indicates good solubility and mobility of the *N*-isopropylacrylamide and PpIX units. However, upon heating, all signals corresponding to PNIPAM shift downfield along with a strong decrease in intensity. This is the result of restricted molecular movement due to aggregation of the thermosensitive *N*-isopropylacrylamide units during phase transitions in aqueous environment, which occur around 38−45 °C. The phase transition temperature (Figure 2c) of the hydrogel was determined to be around 40 °C, which is in good agreement with data from differential scanning calorimetry (DSC) and turbidity testing.

The same procedure was used for the preparation of Pba-PNIPAM and PpIX-DME-PNIPAM. Here a concentration of 3% photosensitizers was used as an optimum concentration for all analyses. Figures S1 and S2 show the FT-IR spectra of Pba-PNIPAM and PpIX-DME-PNIPAM hydrogels, respectively (see Supporting Information). ^{1}H NMR spectra at 25 °C in D_2O for Pba-PNIPAM and PpIX-DME-PNIPAM hydrogels confirmed the formation of the hydrogels (Figures S3 and S4).

UV−Vis and Fluorescence Properties of PS−Nanohydrogels. The UV−vis absorption of free PpIX monomers in H_2O and DMF is shown in Figure 3a. PpIX in MDF is in the monomeric state as indicated by a single, sharp Soret band at 409 nm. In an aqueous environment, PpIX occurs as dimers/aggregates (*vide supra*) and shows two broadened bands at 351 nm with a molar absorption coefficient of $\varepsilon = 0.34 \times 10^5$ M^{-1} cm^{-1} and 450 nm ($\varepsilon = 0.33 \times 10^5$ M^{-1} cm^{-1}). PpIX is a planar molecule which is easily aggregated in aqueous solution. Absorption spectra for PpIX-PNIPAM in water clearly showed that PpIX exists as a monomer in the hydrogel, even at high concentrations (Figure 3c). In contrast to free PpIX in aqueous solution, no significant aggregation was observed in the 2−4 wt % range of PpIX in PNIPAM, as indicated by the sharp Soret band at 405 nm with a high molar absorption coefficient ($\varepsilon = 0.509 \times 10^5$ M^{-1} cm^{-1}).

The fluorescence spectrum of PpIX in DMF showed strong fluorescence at 631 nm (λ_{ex} = 409 nm). For neat PpIX in water (Figure 3b) the fluorescence intensity was weakened accompanied by a blue-shift (λ_{ex} = 409 nm, λ_{em} = 622 nm). In comparison, the fluorescence emission spectra of the PpIX-

DOI: 10.1021/acs.biomac.8b00293
Biomacromolecules 2018, 19, 1592−1601

PNIPAM nanohydrogel for different concentrations of photosensitizers (Figure 3d) revealed an increase in emission intensity (λ_{em} = 632 nm) with increasing concentration of photosensitizer in the nanohydrogel structure. This is further proof that the porphyrin units in the hydrogel structure exist mostly as "monomers", i.e., are spatially well separated and not aggregated. The absence of aggregation is crucial for effective PDT as aggregated PpIX shows low photoactivity. Details of the UV−vis absorption and fluorescence data of the various free PS and PS−hydrogel structures using different solvents are summarized in Table 1.

Table 1. Absorption and Fluorescence Spectroscopic Characteristics of PS and PS−Hydrogels

PS sample	PS (wt %)	Soret bands (nm)	Q-bands (nm)	emission (nm)
free PpIX (H_2O)		351, 450	537, 565, 595, 645	622
free PpIX (DMF)		409	510, 543, 578, 632	631
PpIX-PNIPAM (H_2O)	4	405	510, 543, 582, 647	632
PpIX-PNIPAM (DMF)	4	409	508, 545, 580, 635	633
free Pba (DMF)		409	504, 539, 610, 670	675
Pba-PNIPAM (H_2O)	3	362	558, 610, 673	681
free PpIX-DME (DMF)		404	509, 539, 578, 630	627, 696
PpIX-DME-PNIPAM (H_2O)	3	403	505, 538, 576, 628	625, 690

Pba and PpIX-DME are hydrophobic compounds, insoluble in water or biological media. Clearly, addition of these compounds as copolymers and incorporation into the PNIPAM hydrogel structure result in good water solubility. The fluorescence spectrum of the Pba-PNIPAM hydrogel in H_2O exhibited a fluorescence emission band at 681 nm (λ_{ex} = 409 nm), while PpIX-DME-PNIPAM in water emitted at 623 and 690 nm (λ_{ex} = 404 nm). In all cases the photophysical properties of the PS−hydrogels indicate a significant increase in utility of use of such preparations of PpIX, Pba, and PpIX-DME in biological media as theranostic agents.

Dynamic Light Scattering and Morphological Analysis of the Hydrogels. The structure of the PpIX-PNIPAM hydrogel samples was investigated by SEM (scanning electron microscopy). Figure 4a−c shows SEM images of the surface structure of the freeze-dried PpIX-PNIPAM hydrogel samples. The PpIX-PNIPAM hydrogels are characterized by a highly macroporous, spongelike structure. Most likely the exclusion volume of PpIX provides spatial hindrance during the polymerization and cross-linking process resulting in a more porous structure to the former.[35] The images in Figure 4a−c illustrate that the PpIX-PNIPAM nanohydrogel forms a 3D scaffold with porous layers, in which water can be trapped. Nanoparticles are formed in a submicrometer porous scaffold, and a nanostructured morphology is present in the supramolecular hydrogel. The nanoparticles are uniformly distributed on the surface and aggregation does not occur. In addition, the microporous hydrogel enables PpIX to be delivered effectively to cancer cells as these structures serve as scaffolds for distribution of PpIX as a copolymer in 3D porous systems.

SEM images of Pba-PNIPAM and PpIX-DME-PNIPAM nanohydrogels are shown in Figure S5. The properties of the different PS−hydrogels were also studied by dynamic light scattering (DLS), the size and size distribution of which are summarized in Table 2. DLS analysis for the PpIX-PNIPAM nanohydrogel at different concentrations of PS (2%, 3%, and 4%, w/w) indicated a single peak distribution with a mean diameter of 232 ± 30, 238 ± 15, and 309 ± 25 nm, respectively (Figure 4d−f). Increasing amounts of PpIX conjugated in the hydrogel leads to an increase in size. However, one has to consider that with a significantly higher content of PpIX extended hydrophobic domains are formed slowing down dissolution of the hydrogel in water, and only moderate size growth is observed.[36]

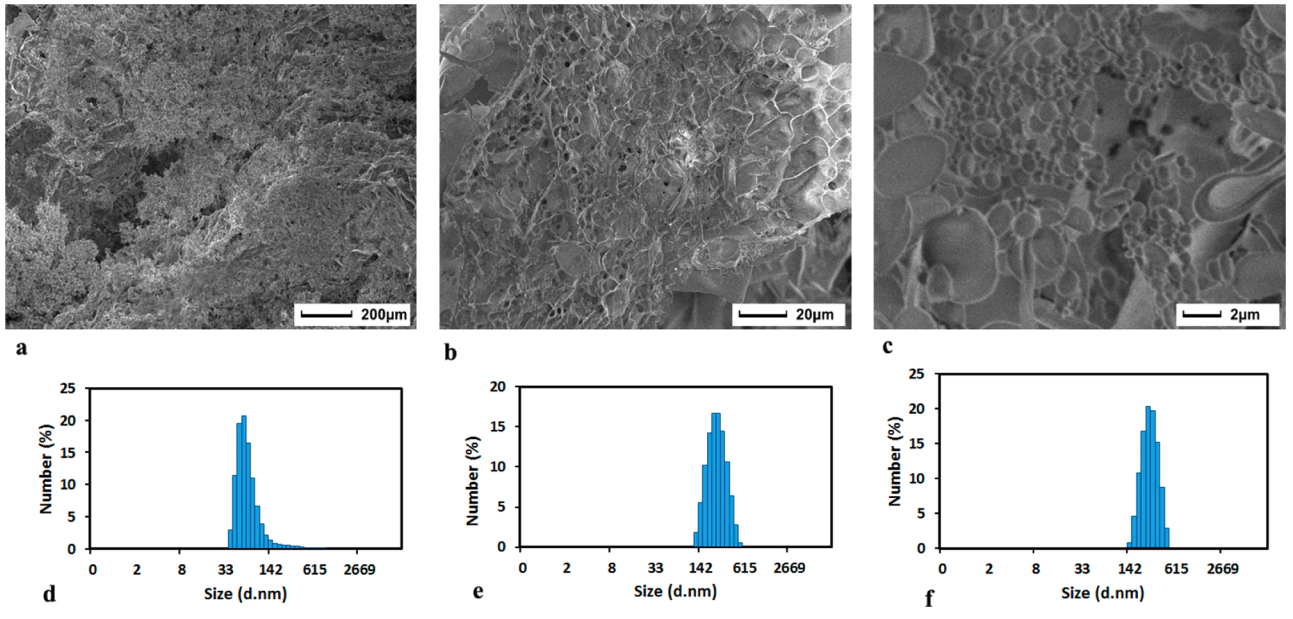

Figure 4. (a, b, c) SEM images of PpIX-PNIPAM hydrogels at different magnifications; (d, e, f) hydrodynamic diameter of PpIX-PNIPAM hydrogel with 2%, 3%, and 4% PS, respectively, as determined by dynamic light scattering.

DOI: 10.1021/acs.biomac.8b00293
Biomacromolecules 2018, 19, 1592−1601

Table 2. Data for Hydrodynamic Diameter (D_h) and Size Distribution (PDI) at Different Concentrations of PpIX in PNIPAM Hydrogels and Data for Pba-PNIPAM and PpIX-DME-PNIPAM (3 wt % PS) As Determined by DLS at 25 °C; Relative Singlet Oxygen Quantum Yield (Φ_Δ) and Efficiency of Singlet Oxygen Delivery (η_Δ) for the Same Systems

PS sample	D_h (nm)	PDI	Φ_Δ	η_Δ
PpIX-PNIPAM 2%	235 ± 5	0.233	n.d.	n.d.
PpIX-PNIPAM 3%	238 ± 6	0.284	1.24	0.69
PpIX-PNIPAM 4%	309 ± 6	0.318	n.d.	n.d.
PpIX-DME-PNIPAM 3%	317 ± 7	0.393	1	0.58
Pba-PNIPAM 3%	283 ± 5	0.326	0.84	0.62

In addition, a well-defined and narrow particle size distribution was found with a mean polydispersity index of 0.272 for the PpIX-PNIPAM nanohydrogel. DLS analysis for Pba-PNIPAM and PpIX-DME-PNIPAM nanohydrogels was only carried out for the sample with 3% of the cross-linker. The size and size distribution of Pba-PNIPAM and PpIX-DME-PNIPAM nanohydrogels showed a single peak distribution with hydrodynamic diameters of 283 ± 13 and 317 ± 15 nm, respectively (Figure S6).

Thermoresponsive Properties. PNIPAM as a thermosensitive polymer for biomedical application is well-studied.[37] Hydrogen bonding between the hydrophilic group (−CONH−) in the PNIPAM chain and the surrounding water molecules results in good solubility. However, hydrophobic interactions involving the isopropyl side group (−CH-$(CH_3)_2$) and water results in precipitation when the temperature nears the lower critical solution temperature (LCST). At this temperature, the polymer faces a phase transition from fully hydrated chains to hydrophobic, collapsed chains.[38] The LCST of pure PNIPAM (32 °C) is lower than the physiological temperature. As a result, *in vivo* applications require a tuning of the LCST to the physiological temperature of 37 °C.[39] Here, *N*-isopropylacrylamide was copolymerized with different porphyrins and chlorophyll monomers to obtain photosensitizer-based hydrogels.

The LCSTs of the three different types of hydrogel under study were determined by measuring the temperature-dependent transmittance (transmittance at 300 nm) and using dynamic differential scanning calorimetry (DSC). Figure 5a shows the temperature-dependent transmittance of the PpIX-PNIPAM hydrogel solution in water. The study indicates that the hydrogel is molecularly soluble and a soluble-to-insoluble transition occurs when the temperature rises above the LCST of 44 °C; this was confirmed by DSC measurements which showed a LCST at 44.52 °C (Figure 5b). The LCSTs of Pba-PNIPAM and PpIX-DME-PNIPAM nanohydrogels were determined as well. The latter (Figure 5d) exhibits a soluble-to-insoluble transition above a LCST of 35 °C. In the case of Pba-PNIPAM, no improvement in the LCST temperature (30 °C, Figure 5c) was observed.

The phase transition of PNIPAM (32 °C)[40] is related to changes of the hydration and dehydration at different temperatures.[41] In the case of PNIPAM/PpIX, PNIPAM/PpIX-DME, and PNIPAM/Pha nanohydrogels the LCSTs are 44, 35, and 30 °C, respectively. A decrease in LCST for PNIPAM/Pha was observed, but the others showed an increase in LCST. Normally, the presence of hydrophobic chains in PNIPAM structures causes a decrease in LCST point due to an

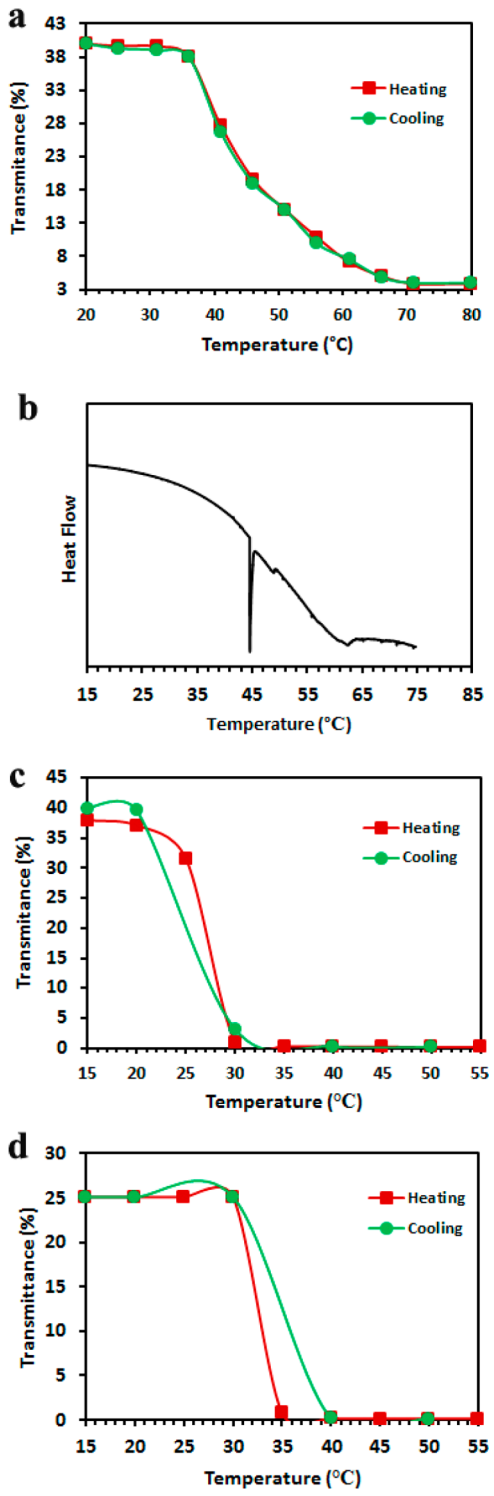

Figure 5. (a) Transmittance versus temperature plots for PpIX-PNIPAM hydrogel (1.35×10^{-5} M) in water. (b) DSC thermogram of PpIX-PNIPAM nanohydrogel in water. (c) Transmittance versus temperature plots for Pba-PNIPAM nanohydrogel and (d) PpIX-DME-PNIPAM nanohydrogel (1.35×10^{-5} M) in water.

increase in hydrophobic interactions.[42] The different LCSTs for PNIPAM/PpIX and PNIPAM/PpIX-DME nanohydrogels can be explained as follows, taking into account that PpIX and PpIX-DME can form two cross-linking bonds with the polymer while Pha can form only one. First, PpIX and PpIX-DME could form hydrophobic cores with a diffuse corona of PNIPAM

DOI: 10.1021/acs.biomac.8b00293
Biomacromolecules 2018, 19, 1592−1601

chains to accelerating the formation of nanohydrogels, and this would isolate the hydrophobic porphyrins from water and repress the hydrophobic effects of the materials.[43] Another aspect is steric hindrance. Because of the densely organized polymeric network, the steric hindrance of the cross-linkers will affect the temperature dependence of the structure.[44] Here, the large planar structure of doubling-linked porphyrins could decrease the tendency of PNIPAM chains to shrink and increase the LCST temperature. Note that a similar trend was also observed in our previous results.[28] PNIPAM/PpIX and PNIPAM/PpIX-DME connect through two points in the hydrogel structure, resulting in a more rigid structure that reduces the freedom of the PpIX and PpIX-DME porphyrins in the hydrogel structure and reduces hydrophobic interactions. The different impact of PpIX and PpIX-DME units is clearly a result of the absence of the hydrophilic carboxylic acid groups in the latter. With only one connecting unit in Pha the overall network might remain more flexible and thus less susceptible to steric effects and the hydrophobic effect of the chlorin unit dominant. Thus, the PpIX-PNIPAM hydrogel is most suitable for biological applications in terms of thermoresponsive behavior.

Singlet Oxygen Measurements. In order to gain a measure on the singlet oxygen generating capacity of the hydrogels $^1O_2$ production was measured by reaction with 1,3-diphenylisobenzofuran (DPBF) using TPP as a standard.[33] The results of the irradiation of the samples in the presence of DPBF (absorption monitored at 417 nm) with time are shown in Figure 6. Figure 6b shows the decrease in DPBF absorption over time for PpIX-PNIPAM, Pba-PNIPAM, and PpIX-DME-PNIPAM nanohydrogels compared to TPP and a blank reference without PS. The efficiency of singlet oxygen delivery (η_Δ) of PpIX-PNIPAM, Pba-PNIPAM and PpIX-DME-PNIPAM nanohydrogels was calculated by eq 1, and the values are summarized in Table 2. The results indicate all PS-conjugated PNIPAM hydrogels produce singlet oxygen efficiently. The singlet oxygen quantum yield of TPP in DMSO is 0.52;[33] PpIX-PNIPAM, Pba-PNIPAM, and PpIX-DME-PNIPAM gave values of 0.69, 0.62, and 0.58 in DMSO, respectively. These are promising values as the individual PS are not very efficient $^1O_2$ generators in water due to aggregation and excited state quenching. Clearly, the nanoporous 3D structure of the hydrogel prevents the aggregation of porphyrins and increases the efficiency of singlet oxygen production in new PNIPAM-based hydrogels. The relative singlet oxygen quantum yields (Φ_Δ) of the hydrogels were calculated from the slope of the DPBF degradation in the presence of TPP as reference and are listed in Table 2.

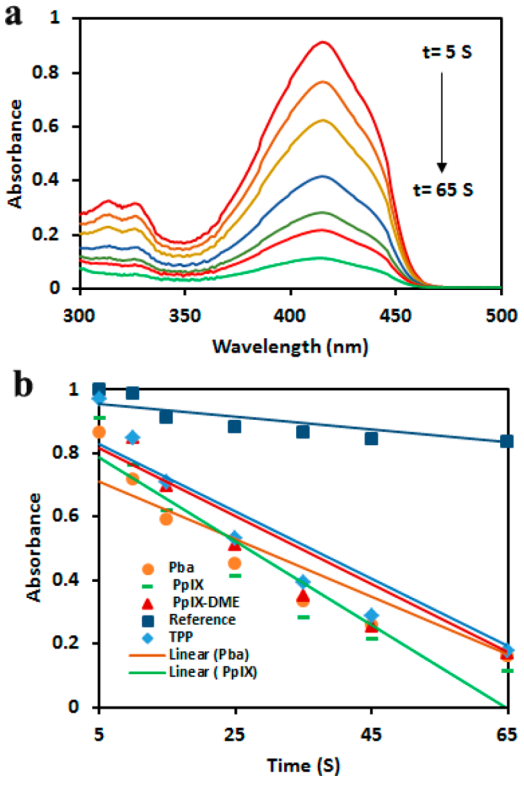

Figure 6. (a) UV−vis spectra of DPBF in the presence of PpIX-PNIPAM 3% hydrogel as a function of laser irradiation time (polychromatic light source). (b) DPBF consumption measured at 417 nm over time in solutions of PpIX-PNIPAM, Pba-PNIPAM, PpIX-DME-PNIPAM, and TPP in DMSO.

***In Vitro* Photocytotoxicity.** Good biocompatibility of the photosensitizer-based hydrogels is important for biomedical applications, and thus the various hydrogel preparations were evaluated for their cytotoxicity using HT-29 cells. Cell viability was measured with the MTT colorimetric assay after 1 h incubation. As shown in Figure 7, the PpIX-PNIPAM hydrogel exhibited excellent biocompatibility; cell viability remained at >90% even at high PS concentrations. Upon irradiation with light, photocytotoxicity occurred, and the cell viability dramatically decreased. The drug dose required to inactivate 90% (LD_{90}) of the HT-29 cells was established as approximately 75 nM. The sharp on/off light dependency of toxicity and excellent LD90 value suggest that this PpIX-PNIPAM hydrogel has significant potential in future studies. The data compare favorably with related studies on using PpIX as photosensitizer *in vitro*.[45,46]

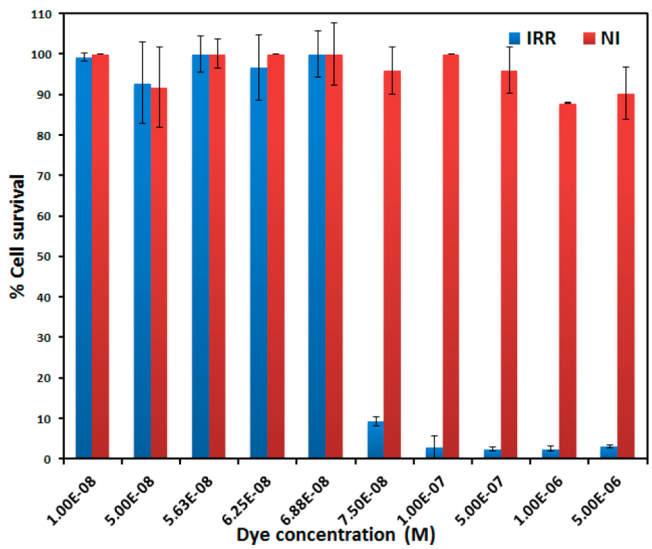

Figure 7. Cell viability after incubation of HT-29 cells with the PpIX-PNIPAM hydrogel (3% PS in hydrogel structure w/w) at different concentrations (1.5×10^{-5}–1.0×10^{-8} M) with irradiation by halogen lamp and without irradiation. Photocytotoxicity is represented as percent cell death after 1 h treatment (illumination, 20 J cm^{-2}, 14 min).

DOI: 10.1021/acs.biomac.8b00293
Biomacromolecules 2018, 19, 1592−1601

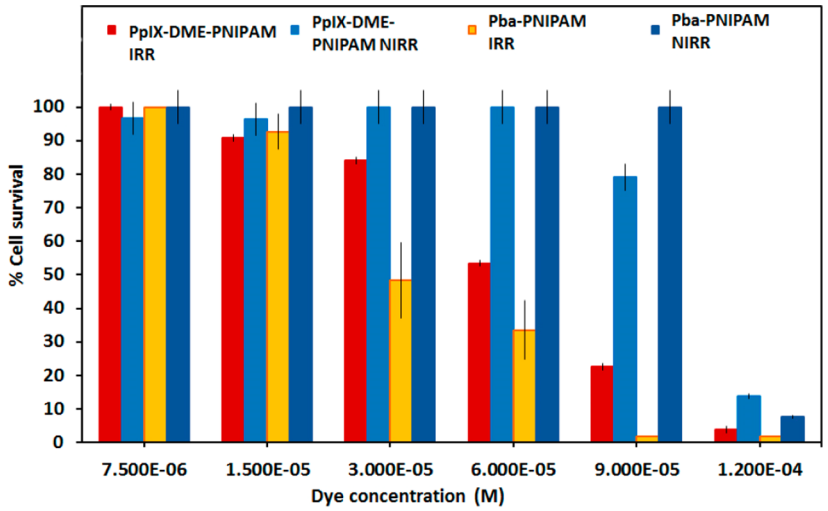

Figure 8. Cell viability after incubation of HT-29 cells with Pba-PNIPAM and PpIX-DME-PNIPAM nanohydrogels (3% PS in hydrogel structure w/w) with HT-29 cells at different concentrations (7.5×10^{-5}–12×10^{-5} M) with irradiation by halogen lamp (IRR) and without irradiation (NIRR). Phototoxicity is represented as the % cell death after 1 h treatment (illumination, 20 J cm^{-2}, 14 min).

Figure 8 shows the cytotoxicity (in the dark) and photocytotoxicity (with irradiation) of Pba-PNIPAM and PpIX-DME-PNIPAM nanohydrogels on HT-29 cells. No significant cytotoxicity was observed for the Pba-PNIPAM nanohydrogel up to 9×10^{-5} M (100% cell viability), and the PpIX-DME-PNIPAM sample did not show any significant cytotoxicity up to 6×10^{-5} M. The results show that dark cytotoxicity of the hydrogels are comparable.

Next, the photocytotoxicity analysis of the Pba-PNIPAM and PpIX-DME hydrogels was evaluated using HT-29 cells (Figure 8). Pba-PNIPAM gave a LD_{90} of 9×10^{-5} M, as opposed to 5×10^{-7} M for Pba alone,[47] while the respective value for PpIX-DME-PNIPAM was determined as 12×10^{-5} M. Additionally, in both cases the efficiency increased gradually with larger concentrations of PS. Interestingly, HT-29 cells treated with PpIX-PNIPAM showed a sharp dose-dependent phototoxicity upon light irradiation. For example, the cell viability upon illumination decreased from 100% to 10% when the PS concentration was increased from 6.8×10^{-8} to 7.5×10^{-8} M. Without irradiation no such effect was observed.

CONCLUSIONS

In summary, poly(*N*-isopropylacrylamide)–PSs (PpIX, Pba, and PpIX-DME) hydrogels have been successfully synthesized with different percentages of photosensitizers as a copolymer in the hydrogel structure. Incorporation of the PS functionalities was easily achieved using the dispersion polymerization method by mixing organic and aqueous solvents. Significantly, spectroscopic data prove that the porphyrin units are incorporated in a "monomeric" manner, without aggregation and thus capable of significant singlet oxygen production. In the case of the PpIX-PNIPAM hydrogel, the absorption spectrum has a sharp Soret band at 405 nm, clearly indicating the absence of aggregation, which is further confirmed by its strong fluorescence emission.

DLS measurements and SEM observation of the hydrogels confirmed the formation of nanohydrogels with diameters of 200–300 nm, i.e., suitable for tissue targeting via the EPR effect. All hydrogels showed a high efficiency of singlet oxygen generation, and notably, the PpIX-PNIPAM hydrogel was biocompatible, with no *in vitro* cytotoxicity in the low micromolar range. Significantly, photocytotoxicity studies demonstrated a dose-dependent generation of singlet oxygen and toxicity with an outstanding LD_{90} of 75 nM for HT-29 cells. Note that many of the other PS (formulations) under study are much less active. In comparison, Pba-PNIPAM and PpIX-DME-PNIPAM nanohydrogels show reasonable biocompatibility and acceptable photocytotoxicity. Clearly, the PpIX-PNIPAM hydrogel has the most potential for *in vivo* investigations and will be the subject of further studies.

All PS–hydrogel preparations showed that using the PS as a chemical cross-linker (copolymer) during hydrogel formation is an effective means (a) to solubilize the photosensitizer for use in aqueous media, (b) to prepare formulations where the PS is effectively monomeric, i.e., photoactive and capable of significant $^1O_2$ production, (c) can be used to modulate the LCST to physiologically relevant parameters, and (d) can yield highly effective light-activated PDT drug candidates.

ASSOCIATED CONTENT

Supporting Information

The Supporting Information is available free of charge on the ACS Publications website at DOI: 10.1021/acs.biomac.8b00293.

FT-IR spectra of Pba, Pba-PNIPAM, PpIX-DME, and PpIX-DME-PNIPAM, ^1H NMR spectra of Pba-PNIPAM and PpIX-DME-PNIPAM, SEM images and DLS results of Pba-PNIPAM and PpIX-DME-PNIPAM, and graphs of singlet oxygen production of TPP, PpIX-PNIPAM, Pba-PNIPAM, PpIX-DME-PNIPAM, and PpIX PNIPAM (PDF)

AUTHOR INFORMATION

Corresponding Author

*E-mail sengem@tcd.ie; Ph +353 (0)1-896-8537; Fax +353 (0) 1 896-8536 (M.O.S.).

ORCID

Ross W. Boyle: 0000-0001-7476-9857

Mathias O. Senge: 0000-0002-7467-1654

Notes

The authors declare no competing financial interest.

DOI: 10.1021/acs.biomac.8b00293
Biomacromolecules 2018, 19, 1592–1601

■ ACKNOWLEDGMENTS

This work was supported by grants from Science Foundation Ireland (IvP 13/IA/1894) and the Research Council of Arak University, Iran.

■ ABBREVIATIONS

DLS, dynamic light scattering; DPBF, 1,3-diphenylisobenzofuran; SEM, scanning electron microscope; LCST, lower critical solution temperature; Pba, pheophorbide a; PDI, polydispersity index; PDT, photodynamic therapy; PNIPAM, poly(*N*-isopropylacrylamide); PpIX, protoporphyrin IX; PpIX-DME, protoporphyrin IX dimethyl ester; PS, photosensitizer.

■ REFERENCES

(1) Dougherty, T. J.; Gomer, C. J.; Henderson, B. W.; Jori, G.; Kessel, D.; Korbelik, M.; Moan, J.; Peng, Q. Photodynamic therapy. *J. Natl. Cancer Inst.* **1998**, *90*, 889−905.

(2) Celli, J. P.; Spring, B. Q.; Rizvi, I.; Evans, C. L.; Samkoe, K. S.; Verma, S.; Pogue, B. W.; Hasan, T. Imaging and Photodynamic Therapy: Mechanisms, Monitoring, and Optimization. *Chem. Rev.* **2010**, *110*, 2795−2838.

(3) Nyman, E. S.; Hynninen, P. H. Research advances in the use of tetrapyrrolic photosensitizers for photodynamic therapy. *J. Photochem. Photobiol., B* **2004**, *73*, 1−28.

(4) Konan, Y. N.; Gurny, R.; Allemann, E. State of the art in the delivery of photosensitizers for photodynamic therapy. *J. Photochem. Photobiol., B* **2002**, *66*, 89−106.

(5) Paszko, E.; Ehrhardt, C.; Senge, M. O.; Kelleher, D. P.; Reynolds, J. V. Nanodrug applications in photodynamic therapy. *Photodiagn. Photodyn. Ther.* **2011**, *8*, 14−29.

(6) Senge, M. O. *m*THPC - A drug on its way from second to third generation photosensitizer? *Photodiagn. Photodyn. Ther.* **2012**, *9*, 170−179.

(7) Senge, M. O.; Radomski, M. W. Platelets, photosensitizers, and PDT. *Photodiagn. Photodyn. Ther.* **2013**, *10*, 1−16.

(8) Peng, Q.; Warloe, T.; Berg, K.; Moan, J.; Kongshaug, M.; Giercksky, K. E.; Nesland, J. M. 5-Aminolevulinic acid-based photodynamic therapy - Clinical research and future challenges. *Cancer* **1997**, *79*, 2282−2308.

(9) Seo, J.; Jang, J.; Warnke, S.; Gewinner, S.; Schöllkopf, W.; von Helden, G. Stacking Geometries of Early Protoporphyrin IX Aggregates Revealed by Gas-Phase Infrared Spectroscopy. *J. Am. Chem. Soc.* **2016**, *138*, 16315−16321.

(10) Rossi, L. M.; Silva, P. R.; Vono, L. R. R.; Fernandes, A. U.; Tada, D. B.; Baptista, M. S. Protoporphyrin IX Nanoparticle Carrier: Preparation, Optical Properties, and Singlet Oxygen Generation. *Langmuir* **2008**, *24*, 12534−12538.

(11) Yano, T.; Uozumi, T.; Kawamoto, K.; Mukada, K.; Onda, J.; Ito, A.; Fujimoto, N. Photodynamic therapy for rat pituitary-tumor *in vitro* and *in vivo* using pheophorbide a and white light. *Lasers Surg. Med.* **1991**, *11*, 174−182.

(12) Ryan, A. A.; Senge, M. O. How green is green chemistry? Chlorophylls as a bioresource from biorefineries and their commercial potential in medicine and photovoltaics. *Photochem. Photobiol. Sci.* **2015**, *14*, 638−660.

(13) Li, W.-T.; Tsao, H.-W.; Chen, Y.-Y.; Cheng, S.-W.; Hsu, Y.-C. A study on the photodynamic properties of chlorophyll derivatives using human hepatocellular carcinoma cells. *Photochem. Photobiol. Sci.* **2007**, *6*, 1341−1348.

(14) Castano, A. P.; Demidova, T. N.; Hamblin, M. R. Mechanisms in photodynamic therapy: Part three- Photosensitizer pharmacokinetics, biodistribution, tumor localization and modes of tumor destruction. *Photodiagn. Photodyn. Ther.* **2005**, *2*, 91−106.

(15) Li, L.; Nurunnabi, M.; Nafiujjaman, M.; Lee, Y.-k.; Huh, K. M. GSH-mediated photoactivity of pheophorbide a-conjugated heparin/gold nanoparticle for photodynamic therapy. *J. Control. Release* **2013**, *171*, 241−250.

(16) Chen, B.; Pogue, B. W.; Hasan, T. Liposomal delivery of photosensitizing agents. *Expert Opin. Drug Deliv.* **2005**, *2*, 477−487.

(17) Martins, J.; Almeida, L.; Laranjinha, J. Simultaneous production of superoxide radical and singlet oxygen by sulphonated chloroaluminum phthalocyanine incorporated in human low-density lipoproteins: Implications for photodynamic therapy. *Photochem. Photobiol.* **2004**, *80*, 267−273.

(18) Roy, I.; Ohulchansky, T. Y.; Pudavar, H. E.; Bergey, E. J.; Oseroff, A. R.; Morgan, J.; Dougherty, T. J.; Prasad, P. N. Ceramic-based nanoparticles entrapping water-insoluble photosensitizing anticancer drugs: A novel drug-carrier system for photodynamic therapy. *J. Am. Chem. Soc.* **2003**, *125*, 7860−7865.

(19) Hone, D. C.; Walker, P. I.; Evans-Gowing, R.; Fitzgerald, S.; Beeby, A.; Chambrier, I.; Cook, M. J.; Russell, D. A. Generation of cytotoxic singlet oxygen via phthalocyanine-stabilized gold nanoparticles: A potential delivery vehicle for photodynamic therapy. *Langmuir* **2002**, *18*, 2985−2987.

(20) Ideta, R.; Tasaka, F.; Jang, W. D.; Nishiyama, N.; Zhang, G. D.; Harada, A.; Yanagi, Y.; Tamaki, Y.; Aida, T.; Kataoka, K. Nanotechnology-based photodynamic therapy for neovascular disease using a supramolecular nanocarrier loaded with a dendritic photosensitizer. *Nano Lett.* **2005**, *5*, 2426−2431.

(21) Li, B.-h.; Moriyama, E. H.; Li, F.-g.; Jarvi, M. T.; Allen, C.; Wilson, B. C. Diblock copolymer micelles deliver hydrophobic protoporphyrin IX for photodynamic therapy. *Photochem. Photobiol.* **2007**, *83*, 1505−1512.

(22) Wieczorek, S.; Schwaar, T.; Senge, M. O.; Börner, H. G. Specific Drug Formulation Additives: Revealing the Impact of Architecture and Block Length Ratio. *Biomacromolecules* **2015**, *16*, 3308−3312.

(23) Eshghi, H.; Sazgarnia, A.; Rahimizadeh, M.; Attaran, N.; Bakavoli, M.; Soudmand, S. Protoporphyrin IX-gold nanoparticle conjugates as an efficient photosensitizer in cervical cancer therapy. *Photodiagn. Photodyn. Ther.* **2013**, *10*, 304−312.

(24) Oh, I.-h.; Min, H. S.; Li, L.; Tran, T. H.; Lee, Y. K.; Kwon, I. C.; Choi, K.; Kim, K.; Huh, K. M. Cancer cell-specific photoactivity of pheophorbide a-glycol chitosan nanoparticles for photodynamic therapy in tumor-bearing mice. *Biomaterials* **2013**, *34*, 6454−6463.

(25) Peppas, N. A.; Hilt, J. Z.; Khademhosseini, A.; Langer, R. Hydrogels in biology and medicine: From molecular principles to bionanotechnology. *Adv. Mater.* **2006**, *18*, 1345−1360.

(26) Gao, D.; Xu, H.; Philbert, M. A.; Kopelman, R. Ultrafine hydrogel nanoparticles: Synthetic approach and therapeutic application in living cells. *Angew. Chem., Int. Ed.* **2007**, *46*, 2224−2227.

(27) Xing, R.-r.; Liu, K.; Jiao, T.-f.; Zhang, N.; Ma, K.; Zhang, R. Y.; Zou, Q. L.; Ma, G.-h.; Yan, X.-h. An Injectable Self-Assembling Collagen-Gold Hybrid Hydrogel for Combinatorial Antitumor Photothermal/Photodynamic Therapy. *Adv. Mater.* **2016**, *28*, 3669−3676.

(28) Belali, S.; Karimi, A. R.; Hadizadeh, M. Novel nanostructured smart, photodynamic hydrogels based on poly(N-isopropylacrylamide) bearing porphyrin units in their crosslink chains: A potential sensitizer system in cancer therapy. *Polymer* **2017**, *109*, 93−105.

(29) Belali, S.; Emandi, G.; Cafolla, A. A.; O'Connell, B.; Haffner, B.; Möbius, M. E.; Karimi, A.; Senge, M. O. Water-soluble, neutral 3,5-diformyl-BODIPY with extended fluorescence lifetime in a self-healable chitosan hydrogel. *Photochem. Photobiol. Sci.* **2017**, *16*, 1700−1708.

(30) Hynninen, P. H.; et al. Chlorophylls 4. Preparation and purification of some derivatives of chlorophylls a and b. *Acta Chem. Scand.* **1973**, *27*, 1771−1780.

(31) Grinstein, M. Studies of protoporphyrin 7. A simple and improved method for the preparation of pure protoporphyrin from hemoglobin. *J. Biol. Chem.* **1947**, *167*, 515−519.

(32) Tada, D. B.; Vono, L. L. R.; Duarte, E. L.; Itri, R.; Kiyohara, P. K.; Baptista, M. S.; Rossi, L. M. Methylene blue-containing silica-coated magnetic particles: A potential magnetic carrier for photodynamic therapy. *Langmuir* **2007**, *23*, 8194−8199.

(33) Korínek, M.; Dědic, R.; Molnár, A.; Svoboda, A.; Hála, J. A comparison of photosensitizing properties of meso-tetraphenylporphin

DOI: 10.1021/acs.biomac.8b00293
Biomacromolecules 2018, 19, 1592−1601

in acetone and in dimethyl sulfoxide. *J. Mol. Struct.* **2005**, *744*, 727−731.
(34) Mosmann, T. Rapid colorimetric assay for cellular growth and survival: Application to proliferation and cytotoxicity assays. *J. Immunol. Methods* **1983**, *65*, 55−63.
(35) Zhang, X. Z.; Yang, Y. Y.; Chung, T. S.; Ma, K. X. Preparation and characterization of fast response macroporous poly(N-isopropylacrylamide) hydrogels. *Langmuir* **2001**, *17*, 6094−6099.
(36) Schlachet, I.; Sosnik, A. Protoporphyrin IX-modified chitosan-g-oligo (NiPAAm) polymeric micelles: from physical stabilization to permeability characterization. *Biomater. Sci.* **2017**, *5*, 128−140.
(37) Halperin, A.; Kröger, M. Thermoresponsive Cell Culture Substrates Based on PNIPAM Brushes Functionalized with Adhesion Peptides: Theoretical Considerations of Mechanism and Design. *Langmuir* **2012**, *28*, 16623−16637.
(38) Taylor, L. D.; Cerankowski, L. D. Preparation of films exhibiting a balanced temperature dependence to permeation by aqueous solutions − a study of lower consolute behavior. *J. Polym. Sci., Polym. Chem. Ed.* **1975**, *13*, 2551−2570.
(39) Taylor, M. J.; Tomlins, P.; Sahota, T. S. Thermoresponsive Gels. *Gels* **2017**, *3*, 4.
(40) Graziano, G. On the temperature-induced coil to globule transition of poly-N-isopropylacrylamide in dilute aqueous solutions. *Int. J. Biol. Macromol.* **2000**, *27*, 89−97.
(41) Schild, H. G. Poly (N-isopropylacrylamide): experiment, theory and application. *Prog. Polym. Sci.* **1992**, *17*, 163−249.
(42) Xia, Y.; Yin, X.; Burke, N. A.; Stöver, H. D. Thermal response of narrow-disperse poly (N-isopropylacrylamide) prepared by atom transfer radical polymerization. *Macromolecules* **2005**, *38*, 5937−5943.
(43) Kujawa, P.; Segui, F.; Shaban, S.; Diab, C.; Okada, Y.; Tanaka, F.; Winnik, F. M. Impact of end-group association and main-chain hydration on the thermosensitive properties of hydrophobically modified telechelic poly (N-isopropylacrylamides) in water. *Macromolecules* **2006**, *39*, 341−348.
(44) Dai, X.-H.; Jin, H.; Yuan, S.-S.; Pan, J.-M.; Wang, X.-H.; Yan, Y.-S.; Liu, D.-M.; Sun, L. Synthesis and characterization of thermosensitive, star-shaped poly (*ε*-caprolactone)-*block*-poly (N-isopropylacrylamide) with porphyrin-core for photodynamic therapy. *J. Polym. Res.* **2014**, *21*, 412.
(45) Tabata, K.; Ogura, S.-i.; Okura, I. Photodynamic Efficiency of Protoporphyrin IX: Comparison of Endogenous Protoporphyrin IX Induced by 5-Aminolevulinic Acid and Exogenous Porphyrin IX. *Photochem. Photobiol.* **1997**, *66*, 842−846.
(46) Zhang, G. D.; Harada, A.; Nishiyama, N.; Jiang, D. L.; Koyama, H.; Aida, T.; Kataoka, K. Polyion complex micelles entrapping cationic dendrimer porphyrin: effective photosensitizer for photodynamic therapy of cancer. *J. Controlled Release* **2003**, *93*, 141−150.
(47) Hajri, A.; Wack, S.; Meyer, C.; Smith, M. K.; Leberquier, C.; Kedinger, M.; Aprahamian, M. *In Vitro* and *In Vivo* Efficacy of Photofrin and Pheophorbide a, a Bacteriochlorin, in Photodynamic Therapy of Colonic Cancer Cells. *Photochem. Photobiol.* **2002**, *75*, 140−148.

DOI: 10.1021/acs.biomac.8b00293
Biomacromolecules 2018, 19, 1592−1601